Forest Ecology and Management 618 (2026) 124029

Contents lists available at ScienceDirect

Forest Ecology and Management

journal homepage: www.elsevier.com/locate/foreco

Framework for commercial thinning assessment with multitemporal lidar and spatially explicit growth simulation

Liam A.K. Irwin [a,*], Nicholas C. Coops [a], Kirk M. Johnson [a], Alexis Achim [b], Ignacio Barbeito [a], Dominik Roeser [a], Catherine Bealle Statland [c]

[a] Department of Forest Resources Management, University of British Columbia, 2424 Main Mall, Vancouver, BC V6T 1Z4, Canada
[b] Département des sciences du bois et de la forêt, Université Laval, 2425 rue de la Terrasse, QC G1V 0A6, Canada
[c] Forest Analysis and Inventory Branch, British Columbia Ministry of Forests, 727 Fisgard Street, Victoria, BC V8W 9C2, Canada

ARTICLE INFO

Keywords:
Forest growth
Commercial thinning
Precision management
Lidar
Drone
Individual tree detection
Growth model

ABSTRACT

Commercial thinning (CT) aims to mitigate inter-tree competition, allow immediate timber recovery, and improve the growth, value, and resilience of residual trees. However, the implementation and assessment of CT is often complicated by costly field plots that may not capture the heterogeneity of pre-treatment and post-treatment CT stands. Field plots may also struggle to quantify CT responses, particularly when sample sizes are small, repeated measurements are not possible, and unthinned controls are not available. To address these issues, we propose a spatial CT assessment framework that employs multitemporal airborne laser scanning, individual tree detection, and a spatially-explicit growth model to quantify CT removals, project long-term CT responses, and compare yield outcomes between thinned and unthinned scenarios. Then, we apply this framework to eight CT stands in British Columbia, Canada (295 ha total; 366,863 lidar-detected trees), model these stands from initial stand ages of 31–40 to age 100, and explore CT impacts on growth, competition, merchantable volume, and piece size. CT treatment intensity was not uniform and varied spatially between and within stands, with mean basal area removals ranging from 23.9% to 42.6%. Under long-term projections, thinned stands yielded 49% more large-log volume (>40 cm diameter) at age 80 (195 vs 131 m^3 ha^{-1}), and unthinned stands maintained higher overall stem volumes with fewer large trees. After accounting for CT removals, cumulative volume growth was similar between thinned and unthinned scenarios. This framework shows promise to support the establishment, monitoring, and enhancement of CT treatments in operational stands.

1. Introduction

Forest management in Canada is shifting from the extensive harvesting of primary forests to the more intensive management of second-growth stands (Barrette et al., 2023; Lieffers et al., 2023). An important silvicultural tool in this transition is commercial thinning (CT), here referring to the removal of commercially viable dominant and co-dominant trees across even-aged plantations with mechanized harvester and forwarder machine sets. CT operations typically cut access trails into contiguous stands and remove individual trees between trails according to machine reach, minimum inter-tree spacing, and retention targets (Bolding et al., 2025; Pavel et al., 2021). By regulating stand density and reallocating growing space to the retained stems, CT aims to concentrate wood production on fewer, larger trees, reduce time to achieve merchantability, and limit growth stagnation and mortality (Binkley et al., 2004; Saarinen et al., 2020; Woodall and Weiskittel, 2021). CT can thereby: provide immediate merchantable timber to mitigate shortages (Pinno et al., 2021), increase stand value with larger trees (Fransson et al., 2020; Hossain et al., 2022; Reid et al., 2025), and accelerate time to merchantability, reducing stand exposure to major risks such as catastrophic wildfire and insect outbreaks (Chagnon et al., 2025a; Coops et al., 2018; Mulverhill et al., 2025). This combination of outcomes make CT a useful response to address imbalanced forest age and size class structures (Griess et al., 2019; Lieffers et al., 2023), while also potentially improving resilience to climatic stressors (Moreau et al., 2022). Despite these benefits, the efficacy of CT is difficult to anticipate. Stand responses can be highly variable, depending on species composition, age, site, history, thinning intensity and timing (Barrette et al., 2023; Bose et al., 2018a, 2018b; Wagle et al., 2023). CT can also introduce risks such as windthrow, residual stem damage, and altered

* Corresponding author.
E-mail address: liam.irwin@ubc.ca (L.A.K. Irwin).

https://doi.org/10.1016/j.foreco.2026.124029
Received 24 April 2026; Received in revised form 12 June 2026; Accepted 13 June 2026

pest and pathogen dynamics (Chagnon et al., 2025a).

The establishment and evaluation of CT is typically informed by stand-level summaries derived from sparse field plots (pre- and post-treatment) which are used to set prescriptions, confirm treatment implementation (e.g., 40% basal area removal), track growth outcomes, and initialize stand-level growth models to assess long-term CT impacts (BC Ministry of Forests, 2025a). Field plots can be simple to establish but may poorly capture pre- and post-treatment heterogeneity and add substantial cost to marginally profitable CT operations (Ahtikoski et al., 2021). These challenges are compounded in BC, where the appropriate timing, age, and intensity of CT are not settled, and there is limited capacity to monitor extensive treatments, quantify growth responses, and iteratively refine CT prescriptions (Halbritter, 2020). Monitoring CT treatments is also required to meet silvicultural audit and certification requirements, particularly when management occurs on public land and CT prescriptions are closely regulated (BC Ministry of Forests, 2025a). Evaluating CT responses is further complicated by the time delay required to assess growth responses on residual trees (e.g., Boivin-Dompierre et al., 2017) and a lack of paired controls to quantify treatment effects in operational stands (Bose et al., 2018a). Anticipating and monitoring CT outcomes requires spatially detailed, tree-level information that conventional field assessments and projection methods do not provide.

Airborne and unmanned-aerial-vehicle (UAV) laser scanning (ALS and ULS) are well suited for the assessment of CT, with advanced object detection methods providing spatially-explicit, tree-level datasets across entire stands (Keefe et al., 2022). Tree detection across laser-scanning datasets (commonly called lidar data) is particularly reliable in even-aged conifer stands (Jakubowski et al., 2013) for dominant and co-dominant trees that are generally the target of CT (Irwin et al., 2025). The direct comparison of trees detected across multiple ALS acquisitions has previously enabled the tracking of harvest events at the individual tree-level (Yu et al., 2004). With wide-area ALS acquisitions now flown on regular 5–10 year intervals for strategic enhanced forest inventories (White et al., 2025) and targeted ULS acquisitions becoming more common, opportunities for tree-level multitemporal analysis of CT and other silvicultural treatments are growing (Goodbody et al., 2024; Tompalski et al., 2021). Tree-level inventories can be further attributed with lidar-derived metrics such as height, crown dimensions, and modeled attributes such as diameter at breast height (DBH) and tree species (Keefe et al., 2022; Puliti et al., 2025). Recent efforts have applied tree-level inventories to initialize spatially explicit growth models to forecast sub-stand development (Chadwick et al., 2025).

While the utility of ALS to derive tree-level inventories is well-established, a standardized framework that applies these data to the specific information needs of CT is lacking. Herein, we present a framework that (i) leverages multitemporal lidar data for tree detection, (ii) uses spatiotemporal matching to evaluate tree removal and retention following CT, and (iii) generates spatially-explicit growth projections under thinned and unthinned scenarios using a tree-level growth simulator (Goudie et al., 2026). This framework operationalizes the extraction lidar data to support pre-treatment CT assessment, post-treatment monitoring (e.g., proportional basal area removal), and the projection of future CT yield and log-size outcomes. These insights can be used to iteratively improve CT treatment designs and enable tracking of realized growth as thinned stands develop. We demonstrate this approach before and after CT across eight stands (295 ha total) in central BC, projecting the growth of detected trees to age 100 under thinned and unthinned scenarios.

2. Materials and methods

2.1. Study Area

The framework was applied in Tree Farm License 52, an area-based forest management tenure located in the Cariboo region of BC. Within this area, a complex of blocks planned for mechanized CT treatments were identified to develop and deploy the CT assessment framework (Fig. 1) in an operational context (Fig. 2). The stands (295 ha total) are typical of second growth forests (i.e. areas regenerated following previous timber harvest) that managers can target with silvicultural interventions like CT to manipulate future growth and generate immediate returns (Griess et al., 2019; Irwin et al., 2025). Between 1982 and 1990 the targeted stands were clearcut and replanted with lodgepole pine (*Pinus contorta Douglas var. latifolia (*Engelm.*)*), Douglas-fir (*Pseudotsuga menziesii var. glauca* (Bessin) Franco), and interior hybrid spruce (*Picea engelmannii* × *glauca* (Moench) Voss). The CT treatments were implemented in 2023 and 2024 when stands were 31–40 years old, following point sample (prism) surveys that assessed tree species composition, stem density, and basal area. Provincial government CT regulations (BC Ministry of Forests, 2025a) and machinery characteristics were used to define silvicultural prescriptions for each stand. Treatment objectives aimed to recover timber by harvesting 5 m wide access trails at 20 m intervals across 25% of the stand area. This design allowed available machinery to reach-in and remove trees between rows with the goal of achieving a minimum inter-tree spacing of 3.5 m. The CT aimed to encourage the development of larger, high-quality stems for final harvests, planned 10–20 years post-treatment.

2.2. Assessment overview

The CT assessment framework proceeds in five steps (Fig. 1).

1. Two lidar point clouds are acquired for each stand: a pre-thinning baseline and a post-thinning acquisition. Field measurements are collected pre-thinning to support lidar-derived inventory development.
2. Individual trees are detected across each acquisition to produce pre- and post-thinning tree lists. Trees are spatially matched to classify detected trees as “removal” or “retention”.
3. Trees are attributed with species labels, DBH, and merchantable volume estimates, based on lidar-derived metrics, a DBH-height model, and tree-level volume models.
4. Retention and removal trees are used to quantify immediate changes from the CT in basal area and inter-tree competition. Detected removal volumes are compared with sawmill-scaled volumes.
5. Thinned (retention trees) and unthinned (all pre-thinning trees) tree lists are initialized at the stand age of thinning and projected to age 100 using a spatially-explicit, tree-level growth model run over 1 ha sub-stand compartments. Comparing the two scenarios enables a spatial evaluation of CT yields and piece-size outcomes.

The following subsections detail each of the steps in our framework.

2.3. Data acquisition

2.3.1. Laser scanning and imagery

ALS data were acquired in June 2021 using a Riegl Q1560 sensor flown at 2300 m above ground, at 82 m s^{-1} speed, with a pulse repetition frequency of 800 kHz, and a swath overlap of 67%, recording up to seven returns per pulse, and resulting in an average point density of 25 points m^{-2} across the study area. ALS data were clipped to the spatial extent of each CT stand boundary to serve as a pre-thinning baseline.

Following CT operations, in 2023 and early 2024, ULS data were acquired in October 2024. ULS data were acquired with a DJI Zenmuse L2 sensor on a DJI Matrice 300 quadcopter UAV flown at 80 m above ground, a speed of 6.2 m s^{-1}, a pulse repetition frequency of 240 kHz, a swath overlap of 75%, and with the sensor set to repetitive scanning mode, resulting in an average point density of ~2500 points m^{-2}. LAS files and ground points were generated in DJI Terra V 4.3.0. A camera on the ULS sensor also collected RGB imagery with the lidar data, with 80% side and 85% forward overlap. Photogrammetric processing of images

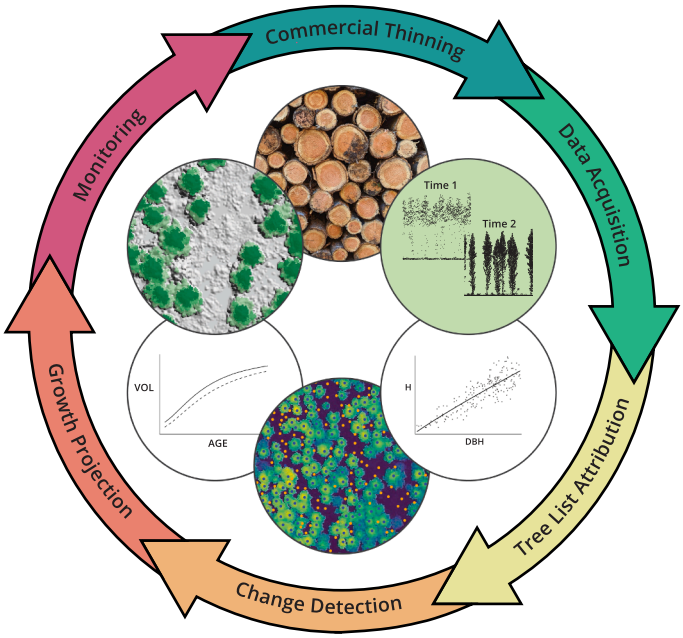

Fig. 1. Overview of the proposed commercial thinning assessment framework. The workflow is driven by (1) multitemporal lidar acquisition before and after thinning, (2) the generation and attribution of thinned and unthinned tree list datasets, (3) detection of changes between these tree lists, (4) projection of future growth, and (5) monitoring of realized changes across thinned stands. The cyclical design reflects the framework's capacity to be applied iteratively, with monitoring outcomes from prior entries informing assessment of subsequent treatments across a stand's silvicultural rotations.

resulted in 1.6 cm orthomosaic imagery across stands post-CT, following workflows in Agisoft Metashape Pro (version 2.1.2) outlined in Irwin et al., (2025).

Differences in lidar data (e.g., ALS vs ULS) require corrections to address differing acquisition characteristics (Næsset, 2009; Roussel et al., 2018, 2017; Tompalski et al., 2019) and spatial alignment to enable precise change detection across derived layers (Riofrío et al., 2022; Yu et al., 2004). To address differences in ground classification each point cloud was height normalized by its own respective ground surface, rather than through the use of a common digital terrain model (Roussel et al., 2020; Tompalski et al., 2019). Alignment was achieved using an initial canopy height model for each acquisition and the high resolution orthomosaic, to determine stable common points in both acquisitions (Yu et al., 2004) and determine an X and Y shift to align ALS point clouds with the ULS. Complex warping was not required to achieve precise alignment due to the high relative positional accuracy of both acquisitions, given the use of survey grade differential GNSS in the ALS acquisitions, and the use of a base station providing continuous real-time-kinematic correction for the imagery and lidar data collected with the UAV.

2.3.2. Field data

Field data included the measurement of DBH and species across 815 trees (>4 cm DBH) in July 2022, collected on nine randomly selected 400 m^2 circular plots located across a subset of the study stands (Irwin et al., 2025). Field heights were measured on a subsample of 196 trees with a Haglöf Vertex, with paired digital calipers for DBH, and a PosTex ultrasonic positioning tool to precisely map stem locations (Lämås, 2010). A Trimble Geo 7X differential GNSS unit was used to geolocate the center of each plot.

2.4. Tree level inventory

Tree-level inventories were derived from both lidar acquisitions by (i) detecting and matching trees to identify removal and retention, (ii) assigning tree species classifications, and (iii) estimating DBH and merchantable stem volumes. These steps are detailed below.

2.4.1. Tree detection and matching

Tree detection and segmentation parameters were applied from a previous study (Irwin et al., 2025) which demonstrated high performance across dominant and co-dominant trees (FSCORE 0.98 and 0.88 respectively) in similar local stand structures and species compositions. Tree tops were detected with the local maxima filter algorithm (2 m diameter circular window, 5 m minimum height) across a 0.25 m canopy height model developed using the lidR package (Roussel et al., 2020) and smoothed with a Gaussian filter. This process was repeated across both the pre-thinning and post-thinning datasets.

To classify tree tops as removal or retention, we implemented nearest neighbor matching. In this approach, T1 trees (pre-thinning) were matched with their two closest Euclidean neighbors (XY) detected in the T2 (post-thinning) dataset. If a unique tree was matched within 2 m, that tree was classified as retention; otherwise, it was classified removal. Following tree matching, pre-thinning height values (2021) were attributed to both timepoints, to avoid incorporating the effect of three years of tree height growth in the estimation of 2024 DBH.

2.4.2. Tree species classification

To describe the post-CT species composition, a random forest classification was trained using tree-level summary metrics derived from the ULS lidar point clouds and RGB imagery and applied to each detected tree with a species label. The two-dimensional extent of each retention tree crown was segmented from the ULS dataset by applying a height-limited watershed algorithm where crown regions are grown from seeds (tree top origin points) across the canopy height model. This approach limits candidate pixels to those within the upper 50% of the tree height to avoid spillover into surrounding vegetation (Grubinger et al., 2023; Irwin et al., 2025). All tree detection and segmentation approaches were applied using the lidR package in R (Roussel et al., 2020). Structural metrics (ULS) and spectral metrics (RGB values from first returns above median height) were summarized for each tree crown point cloud (Appendix: Table A1). Collinear metrics were removed with a Spearman correlation filter (cutoff 0.9; findCorrelation, caret), retaining nine structural and nine spectral predictors. Training data were generated by interpreting tree species on randomly selected

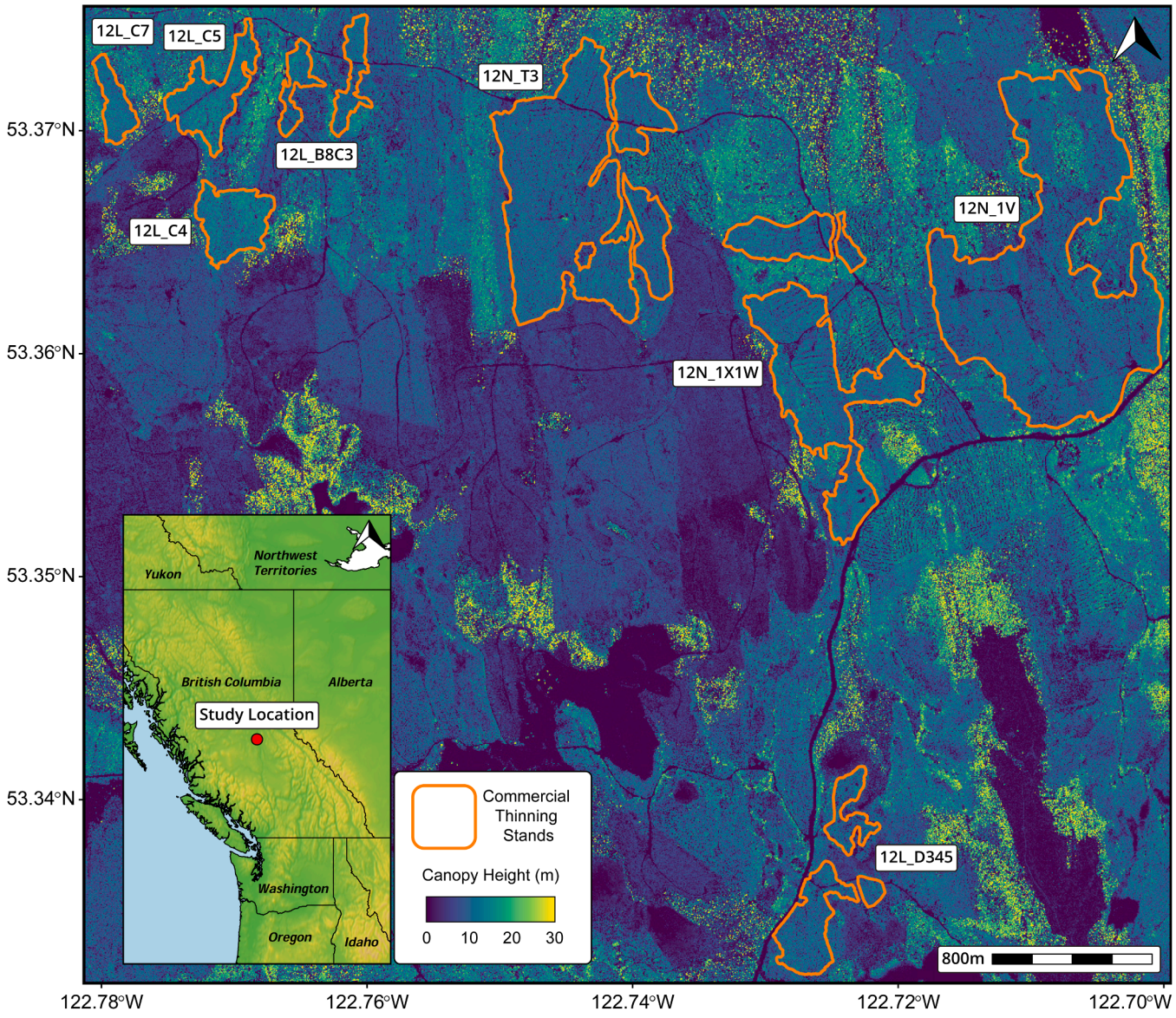

Fig. 2. Overview of the operational commercial thinning stands, totaling 295 ha, evaluated in this application of the assessment framework. Treatment block stand boundaries and labels are overlaid on a canopy height model derived from 2021 airborne laser scanning data, acquired prior to thinning.

400 m^2 tiles of the 1.6 cm RGB orthomosaic, guided by the stem-mapped plots and field visits. Labeled crowns were split 2/3 for training (n = 1532) and 1/3 for testing (n = 786), and a random forest model (caret; ntree = 10,000) was applied to assign species to the ULS trees. Because the pre-CT dataset lacked spectral information, removal trees were assigned species proportionally from the local composition (400 m^2 neighborhood) of retention trees.

2.4.3. Diameter and volume estimation

A single DBH-height model (for all species) was developed from field data to estimate DBH of lidar detected trees before and after CT. This model was built using the subset of tree measurements with a height observation (n = 196), the model form by Cortini et al., (2011) (Equation 1), and nonlinear least squares regression. Predicted DBH and lidar-derived tree height were used to estimate merchantable stem volume (trees > 12.5 cm DBH; 30 cm stump height; 4 cm top diameter) using the species-specific models from Nigh, (2016).

Equation 1:

$$DBH = \beta_0 (HT - 1.29)^{\beta_1}$$

2.5. Change assessment

Immediate CT impacts on stand structure were assessed using the matched and attributed tree lists to evaluate near-term silvicultural objectives (basal area removals, competition reduction) and quantify the spatial heterogeneity of the treatments. This assessment was undertaken at three scales: (i) at the stand-level to represent status quo methods where a post-treatment survey is conducted on a limited set of field plots (BC Ministry of Forests, 2025a), (ii) at a sub-stand level across a 20 m grid, and (iii) at the tree-level to describe shifts in tree distributions and tree attributes following CT.

To describe changes in local above-ground competition between detected dominant and codominant trees, a distance-dependent competition index (CI) was calculated based on tree height, following the approach by Hegyi, (1974). The CI was calculated across a 6 m radius of influence surrounding each target tree, using the TreeCompR package in R (Rieder et al., 2024). For retained trees, CI reduction (%) was calculated as the difference between pre- and post-treatment CI divided by pre-treatment CI.

Detected merchantable stem volumes were summarized for removal trees across each stand and compared with mill scale data that were provided by the forest management company. Information describing exact methodology for sampling was proprietary and unavailable for reference, but generally involves weighing incoming truckloads of sawlogs and pulpwood, scaling a sample of logs, and applying regional weight-to-volume (kg to m^3) models, providing coarse block level values for comparison.

2.6. Growth projection

2.6.1. The Tree and Stand Simulator

Future growth was projected for thinned and unthinned tree lists using the Tree and Stand Simulator (TASS III), a provincial platform that integrates spatially-explicit tree lists (stem maps) into growth modeling for managed stands (Goudie et al., 2026; Penner, 2021). TASS III is an individual-tree, distance-dependent growth model, designed for modeling managed coniferous stands under silvicultural treatments. TASS III includes support for pine and spruce and grows individual trees by accounting for site productivity, light conditions (Brunner, 1998), crown dynamics (Penner, 2021), and the annual allocation of growth to different parts of a tree's bole.

TASS III can be initialized using fully enumerated tree lists with spatial coordinates, species information, height, DBH, age, and establishment type (planted/ingress) (Penner, 2021). TASS III also requires a local estimate of site index (productivity) for each species. In this study, tree list data were derived from lidar-detected trees, and TASS III simulations were modeled using 100 × 100 m (1 ha) sub-stand compartments to minimize edge effects between each compartment and conform with best practices for TASS III use (Goudie et al., 2026). Annual tree list outputs from TASS III were aggregated across a finer 20 × 20 m (400 m^2) assessment grid (Fig. 3). This assessment grid size was chosen to capture spatial heterogeneity within stands, match common specifications of field plots (e.g., BC Ministry of Forests, 2025b), and match the spatial resolution of pixel-based lidar derived enhanced forest inventories (Goodbody et al., 2024; White et al., 2013). Simulations used no operational adjustment factors (OAF1 = OAF2 = 1.00), so projections represented potential growth without influence from biotic or abiotic forest-health factors.

2.6.2. Site index

Species-specific site index (SI) values were calculated for each 100 × 100 m (1 ha) compartment to capture the variability in site productivity across stands (Hawkins et al., 2013). Across each compartment, a 10 × 10 m (100 m^2) sub-grid was used to identify the tallest detected tree for each species in a sub-grid cell, yielding up to 100 dominant tree observations for each species in a compartment. SI values were obtained from species-specific height x age equations in SiteTools

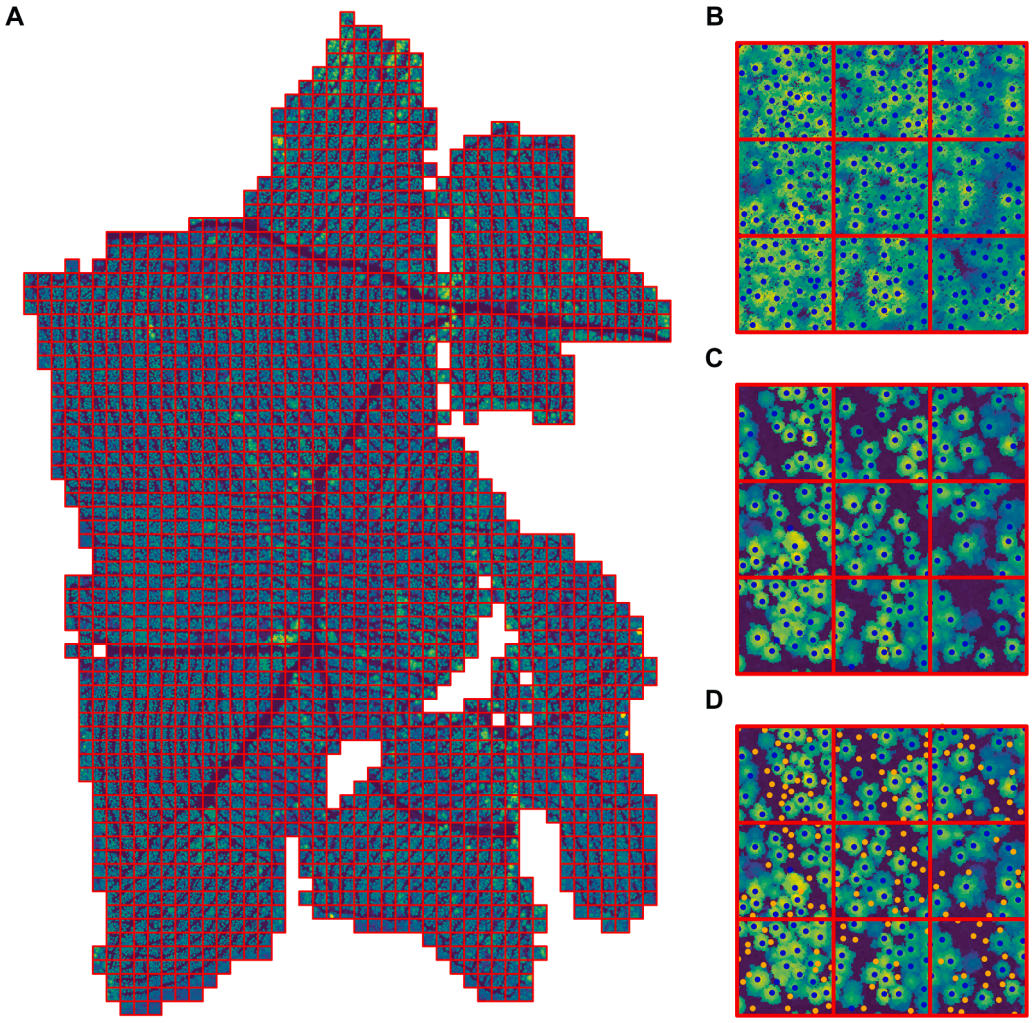

Fig. 3. Example of study block 12N_T3 (79.7 ha) partitioned into a sub-stand assessment grid (400 m^2 cells). A. Entire stand with the assessment grid overlaid on a post-thinning canopy height model. B. Nine assessment grid cells with pre-thinning canopy height model and detected tree tops overlaid. C. Post-thinning canopy height model with detected tree tops. D. Matched tree lists overlaid (blue = retention, orange = removal).

4.3 (BC Ministry of Forests, 2023) and averaged to a single value for each species in a compartment.

2.6.3. Growth simulation approach

With lidar-detected tree lists prepared for each growth compartment under thinned and unthinned scenarios (i.e. tree lists attributed with DBH, coordinates, top height, a classified tree species, and a local site index), each tree list was input into TASS. The current version of TASS III only simulates mixed-species dynamics between white spruce and lodgepole pine. However, the study area also included planted Douglas-fir and naturally occurring broadleaf species in lesser proportions. These species were assigned to a TASS-supported species based on relative similarity in shade tolerance: Douglas-fir was assigned to white spruce (moderately shade tolerant), and broadleaf species (*Populus tremuloides* and *Betula papyrifera*) were assigned to lodgepole pine (shade intolerant). Post-CT detected species proportions are provided in Table 1.

Each stand compartment was initialized at CT age and projected to age 100, beyond the planned harvest age of 10–20 years post-treatment, to explore the development of larger high-value stems and rotation length decisions. Tree-level TASS outputs were generated annually for each compartment and aggregated across the 400 m^2 assessment grids used for change detection, allowing the compilation of merchantable stem volume (m^3 ha^{-1}) across DBH classes (Fig. 3). Merchantable stem volume was also reformulated into cumulative and relative volume growth (CVG and RVG) at the tree- and stand-level to evaluate CT growth rates while accounting for removals following Bose et al., (2018a, 2018b). Cumulative Volume Growth (CVG) was calculated as the sum of standing live merchantable volume plus removals from the CT treatment. Relative Volume Growth (RVG) was calculated as the proportional change (% yr^{-1}) in merchantable live volume across annual timesteps $(V_{t+1} - V_t) / V_t$.

3. Results

3.1. Tree level inventory

The non-linear regression to predict tree DBH (Equation 1) resulted in parameter estimates of $\beta_0 = 1.90$ and $\beta_1 = 0.90$ with a coefficient of determination (R^2) of 0.72 and a root mean squared error (RMSE) of 3.40 cm. Tree species classification achieved 89% overall accuracy on the test set of withheld labeled tree crowns (n = 786). Per-class recall and precision (%) were as follows: lodgepole pine (95.4/88.4), white spruce (90.9/93.3), Douglas-fir (78.3/83.2), and the broadleaf group (93.3/94.9). The top predictor variables determined by the random forest classifier for each tree species are provided in Appendix A: Table A2.

3.2. Structural changes

Across study blocks, the mean basal area removal ranged from 23.9% to 42.6%, while the mean competition index (CI) reduction varied from 26.6% to 45.6%. Within-stand variability in removal, expressed as the standard deviation of basal area removal, and competition reduction (%) ranged from 14.1% to 18.9% and 13.5–17.7%, respectively for all assessment cells (n = 8255) across the eight CT blocks (295 ha). Total lidar-derived removal (merchantable stem volume) aggregated across study blocks (15,386.5 m^3), represented 61.6% of the total scaled mill log volume from the CT operations (24,970.5 m^3). Compared with the sawlog component of scaled loads originating from CT blocks (17,728.9 m^3), the lidar-derived merchantable stem volume accounted for 86.8% of this value. Lidar-derived volumes were lower than scaled sawlog load volumes in seven blocks, 12N_T3 was the only block where the lidar estimate was greater (5192.5 m^3 and 4747.7 m^3) (Table 1).

Spatially, the distribution of the competitive release was concentrated around access trail and roadway edges, decreasing with distance from row. Maps of the two largest CT stands show variability in tree-level reductions of competition index and removal across more heavily thinned and retained areas (Fig. 4).

Cumulative basal area determined by aggregating thinned and unthinned tree lists across 400 m^2 assessment grids enabled comparison of pre- and post-treatment basal area demonstrating variability of removal, and pre-treatment conditions across the stands (Fig. 5). Areas of high basal area removal are evident where access roads and trails were cut, contrasting areas of low or no change present along boundaries and in high retention patches (Fig. 4C).

3.3. Growth projections

Annual TASS tree list outputs for each CT block were aggregated across the 400 m^2 assessment grids (Fig. 3) to describe stand-level projections under the thinned and unthinned scenarios. Merchantable stem volume was projected to be consistently lower across all thinned stands

Table 1
Summary of the eight commercial thinning (CT) blocks assessed before and after thinning from the tree-level remote-sensing inventory: treated area, stand age (2021), lidar-detected tree counts, species proportions of classified trees (spruce (Sx), pine (Pli), Douglas-fir (Fdi), and broadleaf species. (De)). Immediate change represented with pre- (unthinned) versus post-treatment (thinned) basal area and tree-level competition index, with block level total detected merchantable stem volume from lidar-detected trees, and mill-scale values from loaded truck measurements estimating total log volume (sawlog and pulpwood), pulpwood loads in parentheses.

CT Block	Area (ha)	Stand age	Detected trees (n)		Species proportions (%)	Basal area (m^2 ha^{-1})		Competition index		Removal Volume (m^3)	
			Unthinned	**Thinned**		**Unthinned (SD)**	**Thinned (SD)**	**Unthinned (SD)**	**Thinned (SD)**	**Detected**	**Scale Volume (Pulpwood)**
12N_1V	111.4	32	83,845	50,499	40 Sx, 34 Fdi, 15 Pli, 11 De	20.6 (8.3)	12.8 (6.1)	2.13 (0.53)	1.26 (0.42)	5125.1	6553.9 (2407.8)
12N_T3	79.7	31	62,791	35,309	69 Pli, 14 Sx, 9 Fdi, 8 De	21.9 (8.8)	12.6 (5.7)	2.22 (0.49)	1.21 (0.43)	5192.5	4747.7 (2212.5)
12N_1X1W	49.6	32	37,994	23,668	39 Sx, 35 Fdi, 18 Pli, 8 De	20.4 (9.1)	13.0 (5.9)	2.17 (0.48)	1.37 (0.45)	2423.1	3342.9 (1040.7)
12L_D345	17.6	30	16,921	11,609	77 Pli, 13 Fdi, 5 Sx, 5 De	24.2 (12.3)	16.8 (9.3)	2.74 (0.63)	1.89 (0.66)	1000.0	810.7 (262.8)
12L_C5	11.7	40	7807	5781	59 Fdi, 31 Sx, 7 Pli, 3 De	20.9 (9.3)	16.0 (7.4)	1.78 0.39)	1.31 (0.39)	413.9	450.1 (238.6)
12L_C4	10.6	40	8515	5308	46 Sx, 42 Fdi, 6 Pli, 6 De	25.2 (10.0)	16.2 (7.2)	2.26 (0.52)	1.36 (0.43)	664.8	729.6 (329.3)
12L_B8C3	9.3	40	6312	4192	58 Fdi, 24 Sx, 12 Pli, 6 De	17.4 (8.8)	11.9 (6.8)	1.82 (0.46)	1.19 (0.43)	388.3	786.8 (544.8)
12L_C7	4.8	40	3659	2653	75 Sx, 19 Fdi, 4 Pli, 2 De	20.3 (8.6)	15.0 (6.9)	2.02 (0.39)	1.48 (0.37)	178.8	307.2 (205.2)
Total	**294.8**		**227,844**	**139,019**		**21.2 (9.1)**	**13.3 (6.5)**	**2.18 (0.54)**	**1.31 (0.47)**	**15,386.5**	**17,728.9 (7241.6)**

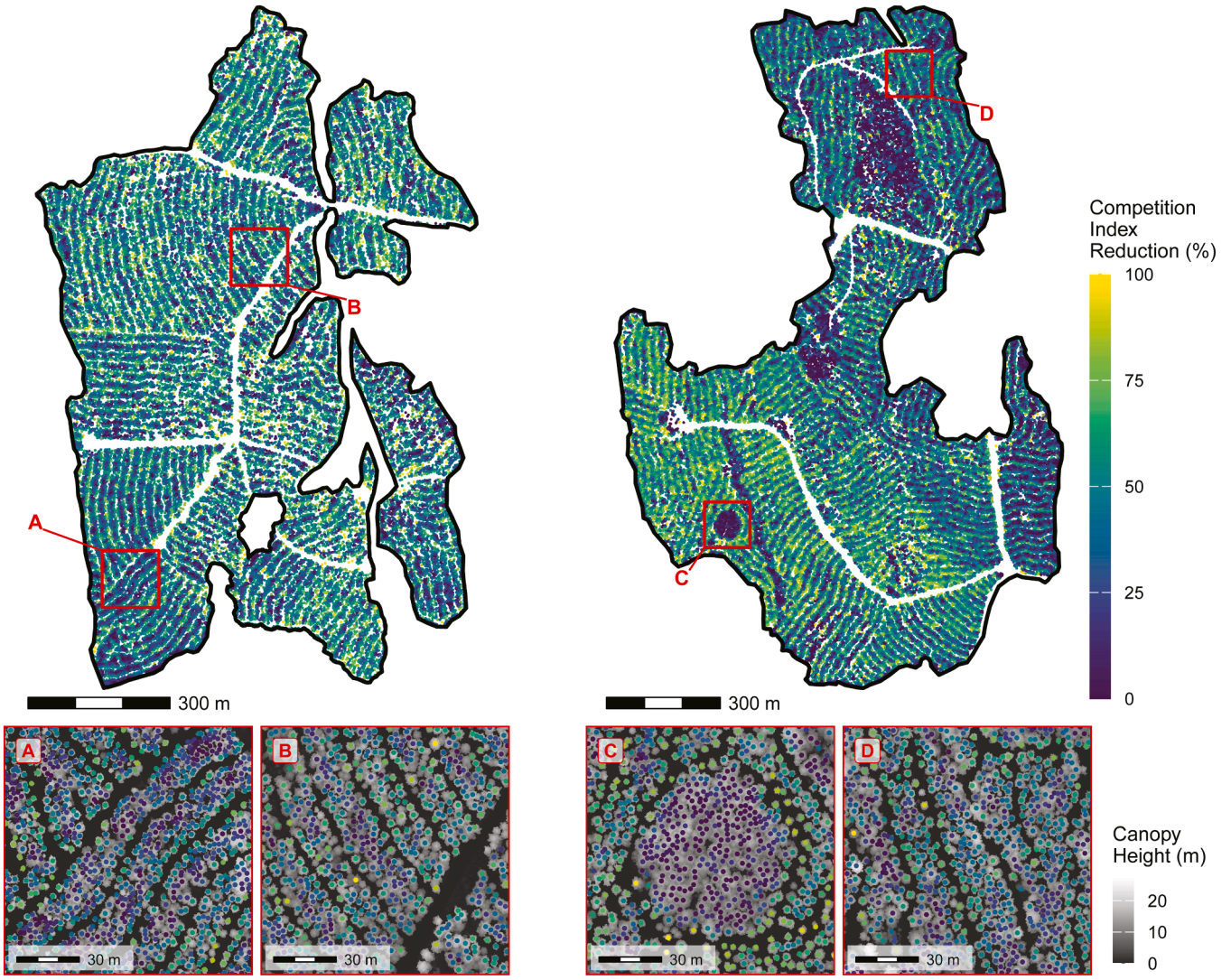

Fig. 4. Maps of retention trees for 12N_T3 (left) and 12N_1V (right), showing individual-tree reductions in a distance-dependent competition index. The index is calculated from the heights of neighboring trees within a 6 m radius of influence, before and after commercial thinning. Inset maps overlay a post-thinning canopy height model (0.25 m resolution) to highlight areas with variable removal and competition reduction.

following CT implementation through to age 100 (Fig. 6). However, large-tree volume (>40 cm DBH) was projected to be higher in thinned stands once modeled trees reached this size class, with an average increase of 49% across the eight stands by age 80 (195 m^3 ha^{-1} vs 131 m^3 ha^{-1}).

Projections of merchantable stem volume aggregated with removals as CVG showed that thinned stands were projected to approach and, in some cases, closely matched the volumes projected across the unthinned stands (Fig. 7). RVG was higher immediately following thinning, with the difference diminishing with increasing stand age as canopy closure occurs across available growing space, following the CT treatment.

Across assessment cells, both scenarios showed a consistent, non-linear increase in total merchantable volume over time (Fig. 8). Thinned cells, however, showed a more concentrated distribution of outcomes than unthinned cells, particularly before age 60. This likely reflects the reduced heterogeneity in stand density after thinning, constraining the range of expected growth outcomes for retention trees.

Growth outputs can be further parsed by size class and presented over time to show recruitment into larger size classes. Here, the mean merchantable stem volume (m^3 ha^{-1}) is presented for trees across DBH size classes for an individual stand (12N_T3). Total volume remained lower in the thinned stand, but the proportion allocated to larger size classes (e.g., > 40 cm) increased around ten years following thinning treatment (Fig. 9). In the unthinned stand, a larger proportion of volume remained in smaller size classes (20–40 cm) through age 100.

4. Discussion

The presented framework integrates multitemporal lidar with spatially-explicit, tree-level growth simulations at the sub-stand level to evaluate CT impacts and forecast future stand development. Detecting and matching trees across timepoints provides immediate insight into CT effects on stand basal area and competition, allowing managers to verify CT prescriptions and silvicultural objectives. Critically, this approach quantifies basal area removals spatially across entire stands, in contrast to monitoring approaches that reflect stand-level values from a limited number of field plots. Initializing CT simulations (pre- and post-treatment) with a spatially-explicit, tree-level growth model (TASS III) also estimates long-term CT responses and changes to stand- and sub-stand growth. This information can help managers iteratively adapt CT treatment designs, better quantify CT treatment responses, and target specific timber-supply objectives (e.g., piece sizes; Lieffers et al., 2023).

Heterogeneity in both pre-thinning structure and post-thinning removal was evident across the CT stands (Fig. 4, Fig. 5). CT responses

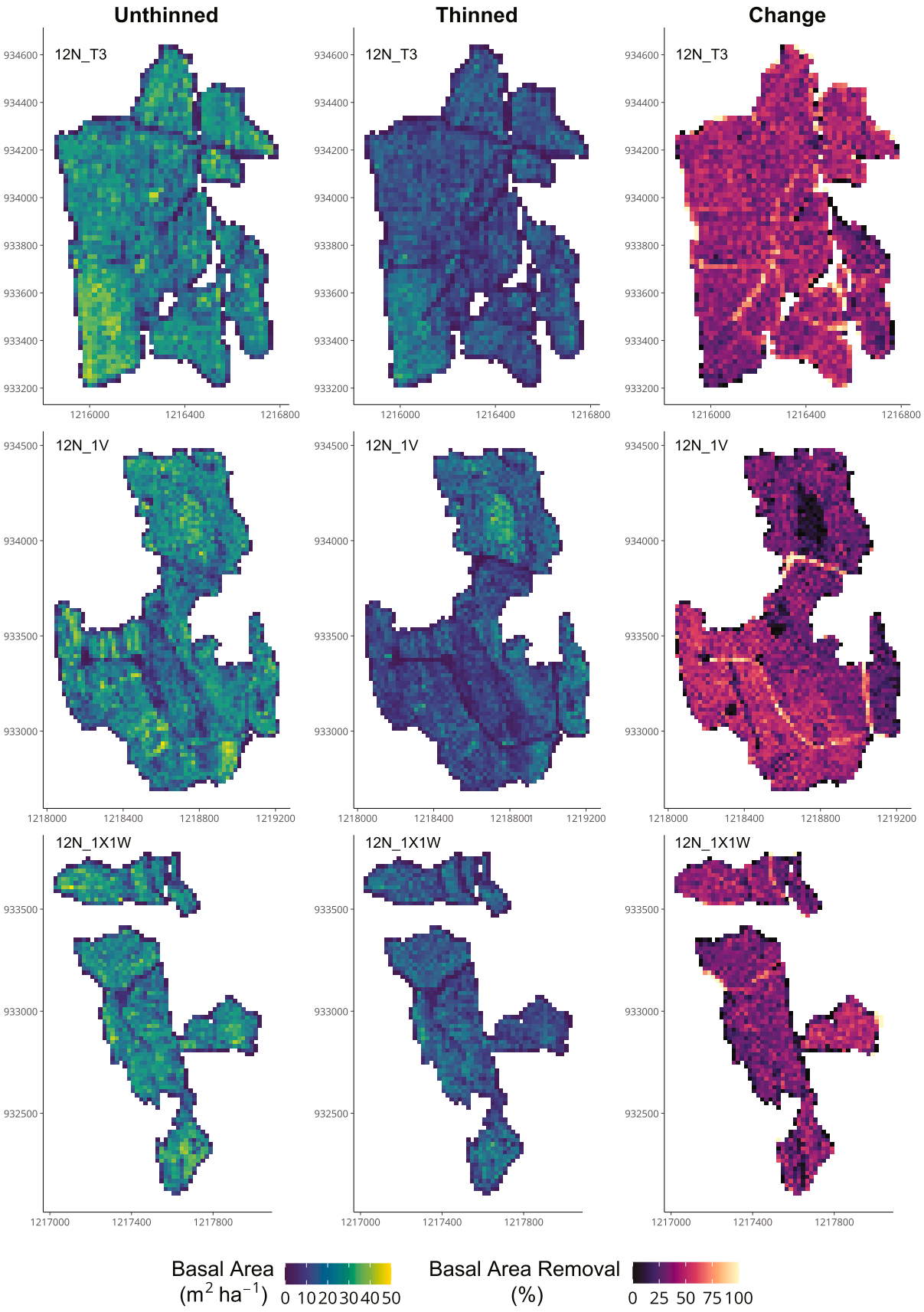

Fig. 5. Spatial distribution of basal area calculated from unthinned and thinned lidar-derived tree lists for the three largest commercial thinning stands: 12N_T3 (top), 12N_1V (middle), and 12N_1X1W (bottom). Cumulative basal area and percent change are presented for trees aggregated across an assessment grid (400 m^2). Hotspots of basal area removal are visible along main roads and trails, alongside high-retention areas and zones of variable initial basal area prior to treatment. Easting and Northing (m) coordinates are displayed for stands as X and Y axes in EPSG 3005 coordinate system.

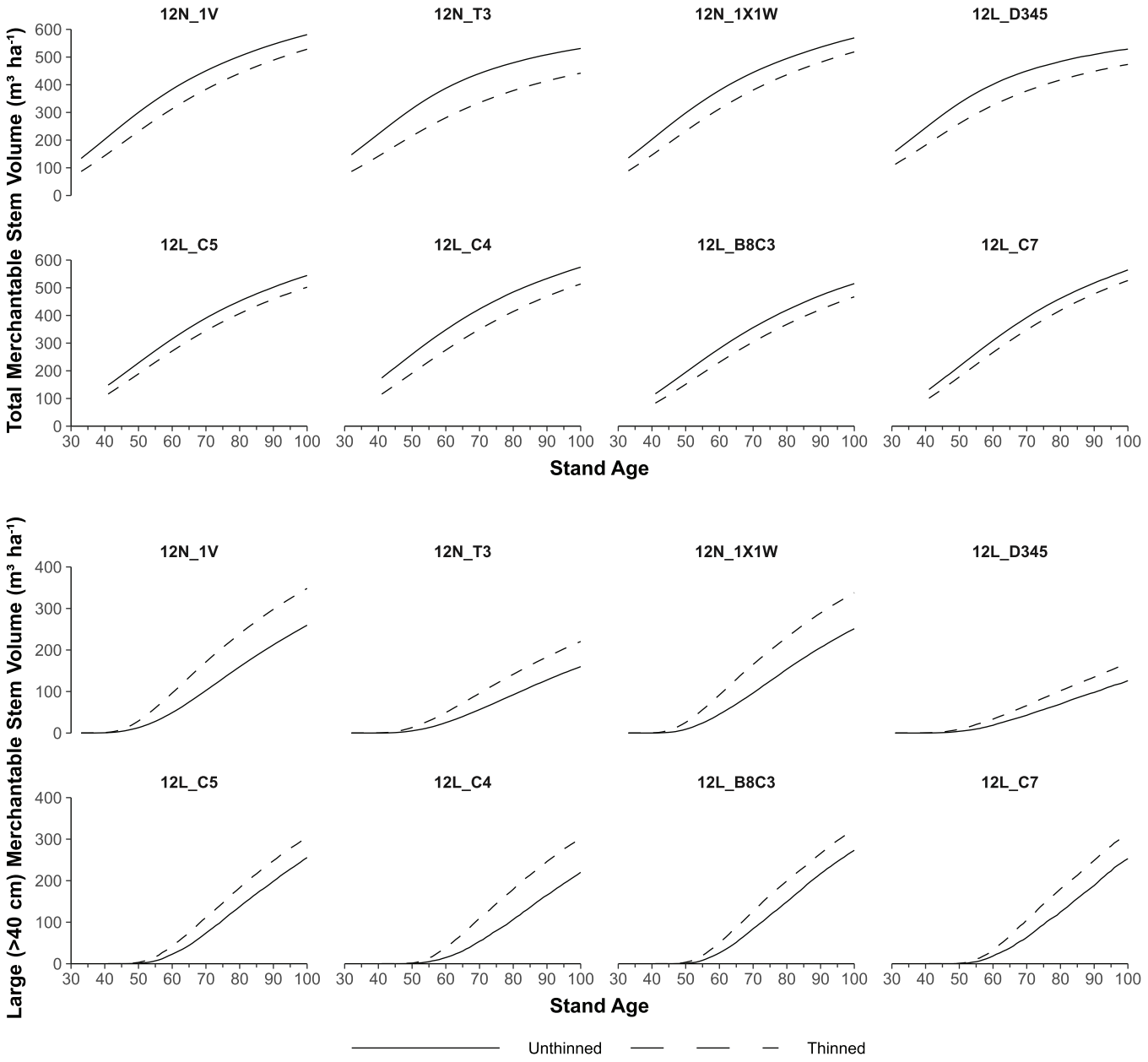

Fig. 6. Projections of total simulated merchantable stem volume (m^3 ha^{-1}) for all trees (top) and large-diameter trees > 40 cm (bottom) across thinned (dashed) and unthinned (solid) stands from age of thinning to age 100. Values are aggregated across trees in all sub-stand growth compartments and expressed on a per-hectare annual basis. Merchantable volumes use a 12.5 cm + diameter utilization standard with a 30 cm stump *height* and 4 cm top diameter.

have been historically evaluated using research plots (e.g., Ara et al., 2024; Boivin-Dompierre et al., 2017; Johnstone and Van Thienen, 2006), expansive silvicultural networks (e.g., Wagle et al., 2023), or simplified scenarios based on synthetic data (e.g. BC Ministry of Forests, 2025a). Instead, this approach captures how stands develop under real, operational treatments measured with wall-to-wall multitemporal lidar. Nevertheless, CT responses remain difficult to evaluate directly, given lag effects (e.g., Boivin-Dompierre et al., 2017), and the absence of experimental controls (e.g., Wagle et al., 2022). This framework supplements existing CT research plots, enhances long-term monitoring, and provides a modeled approximation of an untreated control.

The post-CT structural assessment detected mean basal area removals of 24–43% across the study stands, allowing managers to verify whether CT prescriptions were met and providing a quantitative baseline for subsequent analyses. The distance-dependent competition index closely tracked CT basal area removals (Fig. 4). Furthermore, CT basal area removals and subsequent competition index reductions were concentrated along extraction trails and access roads, consistent with field-based findings that shorter distances to extraction trails (i.e. areas of low competition) increase growth efficiency (Boivin-Dompierre et al., 2017). The assessment of a competition index rather than basal area removal can also help optimize operations for growth response and other objectives (Irwin et al., 2025).

Merchantable removal volumes from lidar data and sawmill scale data agreed fairly well, particularly for the sawlog component alone. Including pulpwood loads dropped agreement from 86.8% to 61.6%. Several factors likely contribute to this gap. The lidar inventory is most reliable for dominant and co-dominant trees (merchantable volume for stems > 12.5 cm diameter), so undetected smaller trees could account for much of the missing pulpwood. Mill-scaled volumes are themselves modeled values with weight-based conversion factors, adding further uncertainty. Unaccounted change in the two growing seasons between

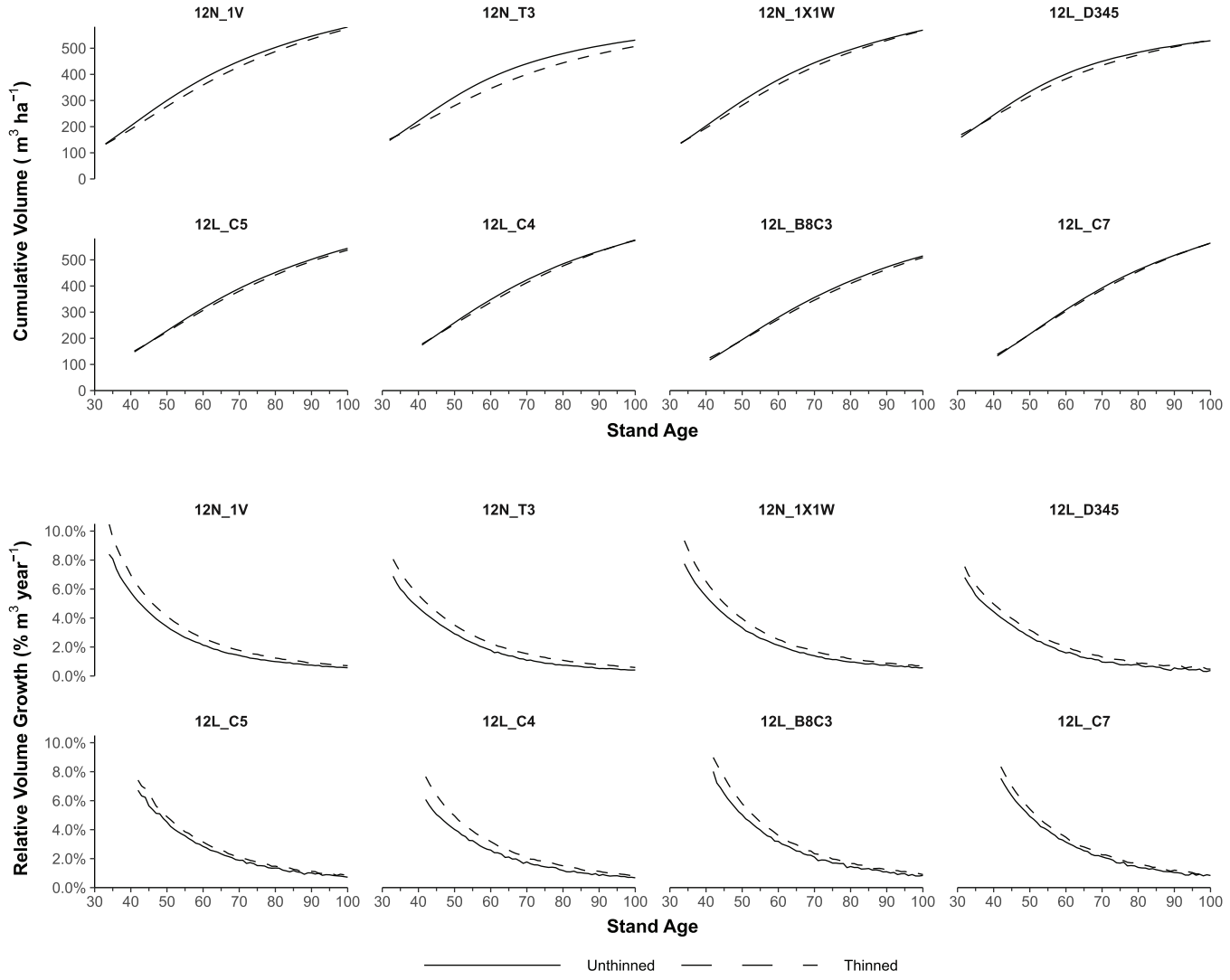

Fig. 7. Mean Cumulative Volume Growth (CVG, m^3 ha^{-1}) and Relative Volume Growth (RVG, % yr^{-1}) across annual simulation timepoints for eight commercial thinning study blocks. Tree lists from unthinned (solid) and thinned (dashed) stands were used to project growth to age 100. Both metrics are calculated from merchantable live standing volume; CVG for thinned stands also includes the contribution from lidar-derived detected removal merchantable volume.

pre-thinning lidar acquisitions and CT operations also contribute to uncertainty. Ideally, a direct validation of the lidar-based approach would use physically scaled log measurements where incoming stems are sampled for volume, rather than weight-derived estimates. Sparks et al. (2024) demonstrated this in a 1.1 ha mixed-conifer stand, validating lidar-derived volume against felled tree measurements and log scaling data that captured 78–91% of field-reference volume. Sparks et al. (2024) also highlighted the uncertainty in weight-to-volume conversion factors and difficulties tracking log loads to specific harvest areas. These issues are compounded across the 295 ha operational scale of this study, where such validation data are not available. Finally, operational data on productivity, such as machine working time and harvester volume obtained from spatially-explicit sensors on equipment, could bolster these evaluations of CT (Lahrsen et al., 2024; Mologni et al., 2024).

Spatially-explicit sub-stand projections of long-term CT responses were also evaluated using annual maps of localized production across the operational stands. Aggregated at the stand-level, these projections of mean stand volume largely followed expected trends post-CT, with lower total merchantable volume growth under thinned conditions before considering removal volume (CVG, Fig. 7). When isolating volumes for large trees (>40 cm DBH), projections indicate additional large log volumes in thinned stands, with 49% greater mean large log volumes by age 80 across the study area (Fig. 6). When paired with information on log prices, piece size specific projections can enable managers to more comprehensively assess the economics of CT operations, which can impact cost benefit analyses, treatment implementations, and foster new management regulations and perspectives regarding CT. The spatial and temporal nature of the sub-stand values can also enable further optimization and prioritization of future entries into treated stands, particularly if discrete regions within a stand are expected to achieve harvest objectives at different times (e.g., Chadwick et al., 2025).

The accelerated recruitment of stems into larger size classes (Fig. 6, Fig. 9) also suggests that thinned stands may reach target piece sizes and merchantable value earlier, potentially advancing the time of final harvest (Hossain et al., 2022). Earlier harvests shorten the period over which stands are exposed to risks such as wildfire and insect attack and may help address timber supply shortages (Lieffers et al., 2023, 2020). Projected growth trajectories were more variable in unthinned stands, and thinned trajectories appeared more concentrated (Fig. 8), producing more homogeneous stand conditions that may be desirable when managing for timber production (Ara et al., 2023).

The framework could be extended with additional laser scanning acquisitions for repeated monitoring over longer periods (Fig. 1),

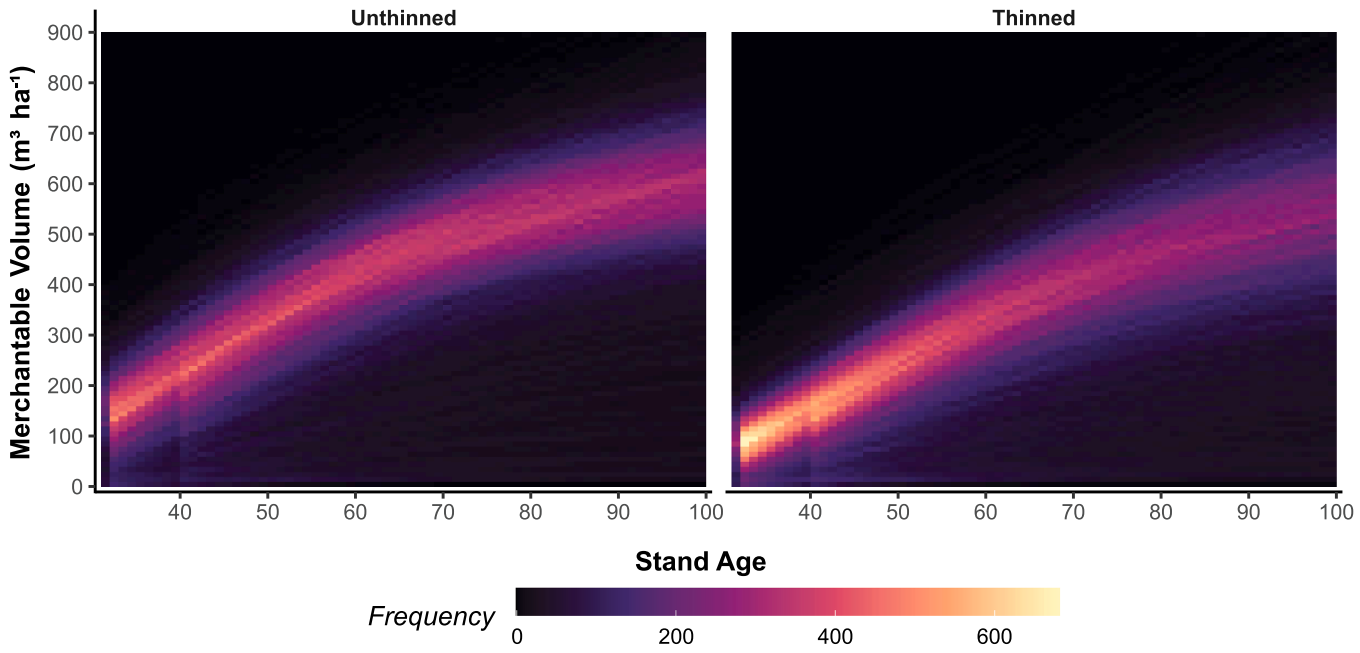

Fig. 8. Frequency distribution of projected tree list growth aggregated across 400 m^2 assessment cells for all eight study commercial thinning stands (295 ha). Values are binned at a 1 year × 10 m^3 ha^{-1} increment for thinned and unthinned tree lists projected to age 100.

particularly once CT release has occurred. This can take the form of repeat tree core, diameter measurements, and additional ALS/ULS acquisitions targeted at tracking crown form which is strongly linked to diameter growth and thinning responses (Ahmed et al., 2024; Bose et al., 2018b; Grubinger et al., 2023; Irwin et al., 2025; Ronoud et al., 2022; Wagle et al., 2023). Establishing operational controls (unthinned areas) alongside these repeat acquisitions could also support growth model development, particularly for regions where existing models are limited (Tompalski et al., 2021) or silvicultural responses are not explicitly modeled (e.g., Weiskittel et al., 2011, p.187).

This framework focuses on stand variables central to active management (basal area, competition, stem volume), but CT also drives broader ecological change (e.g., to soil, hydrology, light conditions) that alters ecosystem services and non-timber values such as understory growth and wildlife habitat; CT also shifts the risk profile and resilience of stands to pests and pathogens (Chagnon et al., 2025a), exposure to wind, and wildfire fuel loads (Bowman et al., 2025). Since the presented approach resolves the position, size, and crown of retained trees, it is well suited to evaluate resilience-focused thinning, and replicating the workflow over time could monitor these risk domains directly. For example, windthrow, pest-induced mortality, and wildfire fuel loads could be detected and tracked before and after disturbance events, allowing for detailed analyses and the refinement of thinning treatments. Finally the framework could be extended to wood-quality modeling, incorporating predictions of silvicultural impacts on product attributes (Drew et al., 2022). For example, CT treatments could be monitored and optimized to generate target wood densities or specific wood products (Mitchell, 1988), and integrated into larger economic modeling frameworks (e.g., Chagnon et al., 2025b; Dura et al., 2025).

The use of a ULS system was essential to fully deploy this framework and enable the monitoring of CT across operational stands. A previously collected ALS dataset was suitable as an initial time step; however, due to prohibitive costs and logistical constraints, a dedicated acquisition of ALS data from manned aircraft immediately following CT is generally not feasible. In contrast, the flexibility of ULS allows acquisitions to be precisely timed with ground operations which can have highly variable timelines, providing a feedback loop to inform operations (Lahrsen et al., 2024). For more intensively managed land-bases operated by centralized or cooperative agencies or governments, targeted ALS coverages could enable wide-area CT evaluation where ULS detail is not required.

This implementation used relatively simple routines for tree detection, segmentation, DBH attribution, and species classification. These approaches were effective in the even-aged, conifer-dominated stands studied here, where CT removals targeted dominant and co-dominant canopy trees (Irwin et al., 2025). DBH was estimated from height with a single allometric model pooled across species, made necessary by a relatively limited field sample. Species-specific DBH-height models built from a larger field datasets would likely improve DBH predictions. In more complex stands with a significant broadleaf component (e.g., Chadwick et al., 2025) or contributions from sub-dominant trees (e.g., Sparks et al., 2024), more robust methods may be required to segment, attribute, and match bitemporal lidar derived tree-lists. Better detection and attribution of suppressed and intermediate trees, alongside species-specific allometry, could improve the reliability of these approaches and extend their application to pre-commercial and lower-canopy thinning

Mixed species stands respond to thinning in complex ways (Pretzsch et al., 2017), the CT responses from this framework could be improved by integrating a growth model with support for Douglas-fir (Swann et al., 2025) and broadleaf species (e.g., Coates et al., 2003). Despite these limitations, TASS III was selected, given its ability to model at the tree-level, acknowledge the spatial variability introduced by CT, and its widespread application for timber supply modeling in BC (e.g., Griess et al., 2019; Penner, 2021). Adding climate sensitivity into yield projections is likely to become important as stands experience changing climate conditions (Metsaranta et al., 2024), inducing drought, higher temperatures, and altered precipitation regimes (Wotherspoon et al., 2024). Tree-level growth models applicable to CT are attempting to incorporate climate variables such as climate moisture index (e.g., Comeau and Bokalo, 2024), annual patterns of temperature and precipitation (e.g., Fortin et al., 2025, 2022), and late frost and drought events (Martinez-Meier et al., 2008). Pending further development, climate sensitive growth models could consider climate impacts on CT removal rates and growth responses, informing climate adaptive silviculture.

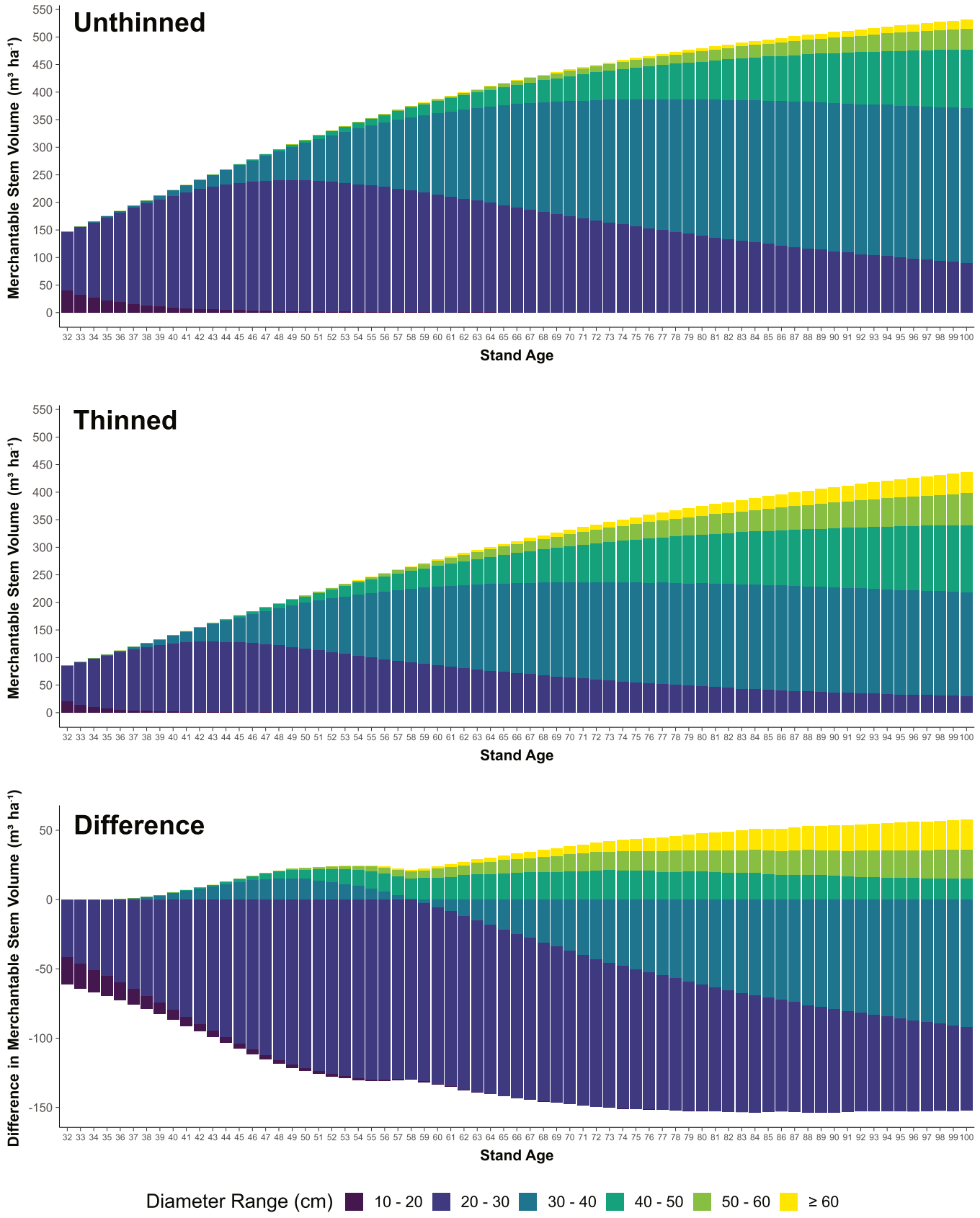

Fig. 9. Projected merchantable stem volume (m^3 ha^{-1}) aggregated across a 79.7 ha stand (12N_T3) and grouped by diameter class. The top panel shows the unthinned stand, the middle panel shows the thinned stand (retention trees only), and the bottom panel shows the difference over time. An additional 65.1 m^3 ha^{-1} of merchantable removal volume was detected across this thinned stand.

5. Conclusions

This study presented an approach to monitor and project the spatiotemporal impacts of commercial thinning (CT) across 295 ha of operationally treated stands by integrating multitemporal lidar with a spatially-explicit tree-level growth model. The framework addresses common bottlenecks that restrict the monitoring of CT outcomes, the refinement of CT prescriptions, and the forecasting of CT responses using sparse field plots that fail to capture CT heterogeneity. The framework also complements existing guidance on CT, provides a quantitative basis to verify operational prescriptions, and supports the ongoing refinement of CT treatment designs. Broader-scale implementation of this framework would require coordinated ALS or ULS acquisitions that are timed with operations, the development of consistent tree detection and attribution routines tested across a wider range of stand types, and the establishment of paired silvicultural controls to support long-term validation of realized growth responses. This framework can support adaptive and precision forest management in delivering more regular, higher-quality timber flows from managed stands.

CRediT authorship contribution statement

Catherine Bealle Statland: Writing – review & editing, Supervision, Software, Resources, Project administration, Methodology. **Dominik Roeser:** Writing – review & editing, Supervision, Conceptualization. **Ignacio Barbeito:** Writing – review & editing, Supervision, Conceptualization. **Alexis Achim:** Writing – review & editing, Supervision, Project administration, Methodology, Funding acquisition, Conceptualization. **Kirk M. Johnson:** Writing – review & editing, Writing – original draft, Validation, Software, Methodology, Investigation, Formal analysis, Data curation, Conceptualization. **Nicholas C. Coops:** Writing – review & editing, Writing – original draft, Supervision, Software, Resources, Project administration, Methodology, Investigation, Funding acquisition, Formal analysis, Data curation, Conceptualization. **Irwin Liam A. K.:** Writing – review & editing, Writing – original draft, Visualization, Validation, Software, Resources, Project administration, Methodology, Investigation, Funding acquisition, Formal analysis, Data curation, Conceptualization.

Declaration of Generative AI and AI-assisted technologies in the writing process

Generative artificial intelligence was used for targeted editorial assistance and code refinement (e.g., improving clarity, spell checking, and debugging errors). All substantive research ideas, methodology, analysis, figures, and results were developed by the authors who thoroughly reviewed and revised any outputs before integration, and take full responsibility for all manuscript content

Declaration of Competing Interest

The authors declare that they have no known competing financial interests or personal relationships that could have appeared to influence the work reported in this paper.

Acknowledgments

Access to and guidance in applying the Tree and Stand Simulator III model was provided by the Forest Analysis and Inventory Branch of the British Columbia Ministry of Forests. Staff at the forest management company West Fraser Quesnel provided access to the study sites, as well as stand-level information and scaled log volumes associated with the CT treatments, as well as valuable context that guided the development of research questions and methods.

This research was conducted as part of the Silva21 Alliance Grant Project (NSERC ALLRP 556265–20) funded by the Natural Sciences and Engineering Research Council of Canada led by Dr. Alexis Achim. Additional funding was provided through postgraduate research scholarships to Liam A. K. Irwin (NSERC PGS-D 579629–2023)

Appendix A

Appendix Table A1
Individual tree crown metrics calculated from lidar point clouds and red-green-blue (RGB) imagery for tree species classification

Metric Category		Summary Statistics	Metric Name	Reference
Structural (Point Cloud)	Height Metrics	100th, 99th, 75th,50th,25th	ZQ100, ZQ99, ZQ75, ZQ50, ZQ25	(Holmgren and Persson, 2004)
	Return Metrics	Number of returns	n_R1, n_R2, n_R3, n_R4, n_R5	(Brandtberg, 2007)
	Shape metrics	Crown Relief Ratio, Percentage of points above 2 m	CRR, pzabove2	(Parker and Russ, 2004)
	Variability metrics	Shannon entropy, Skewness, Coefficient of variation.	Z_entropy, Z_skew, CV_Z	(Brandtberg, 2007; Li et al., 2013)
Spectral (RGB)	Reflectance Values	Mean, standard deviation	R, G, B	
	Chromatic Coordinates	Mean, standard deviation	RCC, GCC, BCC	(Sonnentag et al., 2012)
	Hue and Brightness	Mean, standard deviation	hue, brightness, saturation	(Onishi and Ise, 2021)

Appendix Table A2
Relative importance of the top five variables selected by the random forest classifier for each tree species group

Variable	Douglas-fir	Lodgepole pine	White spruce	Broadleaf
Saturation (mean)	75.06	96.09	100.00	88.51
Saturation (SD)	38.40	59.63	28.15	20.35
R_mean	32.27	51.36	38.31	59.28
B_sd	48.78	47.36	89.48	17.78

(*continued on next page*)

Appendix Table A2 (*continued*)

Variable	Douglas-fir	Lodgepole pine	White spruce	Broadleaf
G_sd	38.27			
B_mean				23.79
GCC_mean		47.87		
Hue_sd			30.07	

Data availability

Data will be made available on request.

References

Ahmed, S., Hilmers, T., Uhl, E., Jacobs, M., Bohnhorst, L., Kolisnyk, B., Del Río, M., Pretzsch, H., 2024. Neighborhood competition modulates the link between crown structure and tree ring variability in monospecific and mixed forest stands. For. Ecol. Manag. 560, 121839. https://doi.org/10.1016/j.foreco.2024.121839.

Ahtikoski, A., Laitila, J., Hilli, A., Päätalo, M.-L., 2021. Profitability of the first commercial thinning, a simulation study in Northern Finland. Forests 12, 1389. https://doi.org/10.3390/f12101389.

Ara, M., Pinno, B.D., Scaria, F., Froese, R.E., Bokalo, M., 2023. Thinning increases individual tree growth while reducing the growth heterogeneity of lodgepole pine. Forests 14, 1091. https://doi.org/10.3390/f14061091.

Ara, M., Pinno, B.D., Scaria, F., Froese, R.E., 2024. Precommercial thinning but not commercial thinning increases the merchantable and large sawlog volume production of lodgepole pine on fair sites. For. Sci. 70, 376–384. https://doi.org/10.1093/forsci/fxae025.

Barrette, J., Achim, A., Auty, D., 2023. Impact of intensive forest management practices on wood quality from conifers: literature review and reflection on future challenges. Curr. For. Rep. 9, 101–130. https://doi.org/10.1007/s40725-023-00181-6.

BC Ministry of Forests, 2023. Site index tools (SiteTools) Version 4.3.

BC Ministry of Forests, 2025a. Thinning Guidance for British Columbia 2025 (Technical Report). Ministry of Forests. Office of the Chief Forester, Victoria, BC.

BC Ministry of Forests, 2025b. Provincial Monitoring British Columbia: Ground Sampling Procedures (Report No. Version 4.1). Forest Analysis and Inventory Branch, Victoria, BC.

Binkley, D., Stape, J.L., Ryan, M.G., 2004. Thinking about efficiency of resource use in forests. For. Ecol. Manag. 193, 5–16. https://doi.org/10.1016/j.foreco.2004.01.019.

Boivin-Dompierre, S., Achim, A., Pothier, D., 2017. Functional response of coniferous trees and stands to commercial thinning in eastern Canada. For. Ecol. Manag. 384, 6–16. https://doi.org/10.1016/j.foreco.2016.10.024.

Bolding, M.C., Conrad, J.L., Eliasson, L., Spinelli, R., Magagnotti, N., Miller, T.R., Mapatunage, H., 2025. The evolution and expansion of cut-to-length harvesting systems beyond scandinavia: challenges and opportunities in Central and Southern Europe and North America. Curr. For. Rep. 11, 24. https://doi.org/10.1007/s40725-025-00256-6.

Bose, A.K., Weiskittel, A., Kuehne, C., Wagner, R.G., Turnblom, E., Burkhart, H.E., 2018a. Does commercial thinning improve stand-level growth of the three most commercially important softwood forest types in North America? For. Ecol. Manag. 409, 683–693. https://doi.org/10.1016/j.foreco.2017.12.008.

Bose, A.K., Weiskittel, A., Kuehne, C., Wagner, R.G., Turnblom, E., Burkhart, H.E., 2018b. Tree-level growth and survival following commercial thinning of four major softwood species in North America. For. Ecol. Manag. 427, 355–364. https://doi.org/10.1016/j.foreco.2018.06.019.

Bowman, D.M.J.S., Weston, E., Nichols, S.C., Williamson, G.J., Prior, L.D., 2025. Impacts of commercial thinning on stand demography, fuel loads, microclimate and fire behaviour in Eucalyptus delegatensis forest in eastern Tasmania. For. Ecol. Manag. 596, 123054. https://doi.org/10.1016/j.foreco.2025.123054.

Brandtberg, T., 2007. Classifying individual tree species under leaf-off and leaf-on conditions using airborne lidar. ISPRS J. Photogramm. Remote. Sens. 61, 325–340. https://doi.org/10.1016/j.isprsjprs.2006.10.006.

Brunner, A., 1998. A light model for spatially explicit forest stand models. For. Ecol. Manag. 107, 19–46. https://doi.org/10.1016/S0378-1127(97)00325-3.

Chadwick, A.J., Coops, N.C., Johnson, K.M., Bater, C.W., Martens, L.A., Röeser, D., White, B., 2025. A remote sensing methodology for sub-stand growth and yield projection of post-harvest forest regeneration. For. Int. J. For. Res. 98, 454–463. https://doi.org/10.1093/forestry/cpae051.

Chagnon, C., Dumont, S., Morin-Bernard, A., Jactel, H., Achim, A., Moreau, G., 2025a. Potential of thinning to increase forest resilience and resistance to drought, pest, windstorm and fire: a meta-analysis. For. Ecol. Manag. 590, 122788. https://doi.org/10.1016/j.foreco.2025.122788.

Pretzsch, H., Forrester, D.I., Bauhus, J. (Eds.), 2017. Mixed-Species Forests. Springer, Berlin, Germany. https://doi.org/10.1007/978-3-662-54553-9.

Chagnon, C., Moreau, G., Soro, A., Bombardier-Cauffopé, C., Baby-Bouchard, E., Chamberland, V., Barrette, J., Gélinas, N., Duchesne, I., Lenz, P., Bousquet, J., Achim, A., 2025b. A comprehensive framework to evaluate the financial impacts of genetic improvement on wood products from planted forests. Can. J. For. Res. 55, 1–15. https://doi.org/10.1139/cjfr-2024-0057.

Coates, K.D., Canham, C.D., Beaudet, M., Sachs, D.L., Messier, C., 2003. Use of a spatially explicit individual-tree model (SORTIE/BC) to explore the implications of patchiness in structurally complex forests. For. Ecol. Manag. 186, 297–310. https://doi.org/10.1016/S0378-1127(03)00301-3.

Comeau, P.G., Bokalo, M., 2024. Aspen and spruce densities affect tree size, future stand volume, and aboveground carbon following precommercial thinning. Forests 15, 223. https://doi.org/10.3390/f15020223.

Coops, N.C., Hermosilla, T., Wulder, M.A., White, J.C., Bolton, D.K., 2018. A thirty year, fine-scale, characterization of area burned in Canadian forests shows evidence of regionally increasing trends in the last decade. PLOS One 13, e0197218. https://doi.org/10.1371/journal.pone.0197218.

Cortini, F., Filipescu, C.N., Groot, A., MacIsaac, D.A., Nunifu, T., 2011. Regional models of diameter as a function of individual tree attributes, climate and site characteristics for six major tree species in Alberta, Canada. Forests 2, 814–831. https://doi.org/10.3390/f2040814.

Drew, D.M., Downes, G.M., Seifert, T., Eckes-Shepard, A., Achim, A., 2022. A review of progress and applications in wood quality modelling. Curr. For. Rep. 8, 317–332. https://doi.org/10.1007/s40725-022-00171-0.

Dura, H., Fortin, M., Achim, A., 2025. Cutting through market trends: the impact of macroeconomy, COVID-19 pandemic, and climate-related disasters costs on wood product prices in North America. Can. J. For. Res. 55, 1–11. https://doi.org/10.1139/cjfr-2025-0001.

Fortin, M., Riofrío, J., De Melo, L.C., Ashiq, M.W., Sharma, M., Howard, C., Eskelson, B. N.I., 2025. Climate-sensitive models of tree mortality based on lifetime analysis and irregular permanent-plot remeasurements. Can. J. For. Res. 55, 1–15. https://doi.org/10.1139/cjfr-2024-0205.

Fortin, M., Sattler, D., Schneider, R., 2022. An alternative simulation framework to evaluate the sustainability of annual harvest on large forest estates. Can. J. For. Res. 52, 704–715. https://doi.org/10.1139/cjfr-2021-0255.

Fransson, P., Franklin, O., Lindroos, O., Nilsson, U., Brännström, Å., 2020. A simulation-based approach to a near-optimal thinning strategy: allowing harvesting times to be determined for individual trees. Can. J. For. Res. 50, 320–331. https://doi.org/10.1139/cjfr-2019-0053.

Goodbody, T.R.H., Coops, N.C., Irwin, L.A.K., Armour, C.C., Saunders, S.C., Dykstra, P., Butson, C., Perkins, G.C., 2024. Integration of Airborne Laser Scanning data into forest ecosystem management in Canada: current status and future directions. For. Chron. 100, 238–258. https://doi.org/10.5558/tfc2024-014.

Goudie, J.W., Cameron, I.R., Statland, C.B., Polsson, K.R., Parish, R., Stearns-Smith, S., Lucca, C.M.D., 2026. Development of the Tree and Stand Simulator (TASS) Version 3.0 (Technical Report No. 155). Province of BC, Victoria, BC.

Griess, V.C., Man, C.D., Polinko, A.D., Spies, J., 2019. Mitigating midterm timber supply shortage using commercial thinning operations. A case study from British Columbia, Canada. For. Ecol. Manag. 443, 1–18. https://doi.org/10.1016/j.foreco.2019.04.003.

Grubinger, S., Coops, N.C., O'Neill, G.A., 2023. Picturing local adaptation: spectral and structural traits from drone remote sensing reveal clinal responses to climate transfer in common-garden trials of interior spruce (Picea engelmannii × glauca). Glob. Change Biol. 29, 4842–4860. https://doi.org/10.1111/gcb.16855.

Halbritter, A., 2020. An economic analysis of thinning intensity and thinning type of a two-tiered even-aged Forest stand. For. Policy Econ. 111, 102054. https://doi.org/10.1016/j.forpol.2019.102054.

Hawkins, C.D.B., Dhar, A., Bittencourt, E., 2013. Improving site index estimates for pine and spruce plantations: a case study in the sub-boreal spruce zone in British Columbia. For. Sci. Technol. 9, 51–58. https://doi.org/10.1080/21580103.2012.759160.

Hegyi, F., 1974. A simulation model for managing jack-pine stands. In: Fries, J. (Ed.), Growth Models for Tree and Stand Simulation, Research Notes, 30. Royal College of Forestry, Stockholm, Sweden, pp. 74–90.

Holmgren, J., Persson, Å., 2004. Identifying species of individual trees using airborne laser scanner. Remote. Sens. Environ. 90, 415–423. https://doi.org/10.1016/S0034-4257(03)00140-8.

Hossain, K.L., Lieffers, V.J., Pinno, B.D., 2022. Thinning to meet sawlog objectives at shorter rotation in lodgepole pine stands. Can. J. For. Res. 52, 940–950. https://doi.org/10.1139/cjfr-2022-0006.

Irwin, L.A.K., Coops, N.C., Riofrío, J., Grubinger, S.G., Barbeito, I., Achim, A., Roeser, D., 2025. Prioritizing commercial thinning: quantification of growth and competition with high-density drone laser scanning. For. Int. J. For. Res. 98, 293–307. https://doi.org/10.1093/forestry/cpae030.

Jakubowski, M., Li, W., Guo, Q., Kelly, M., 2013. Delineating individual trees from lidar data: a comparison of vector- and raster-based segmentation approaches. Remote. Sens. 5, 4163–4186. https://doi.org/10.3390/rs5094163.

Johnstone, W.D., Van Thienen, F., 2006. A Summary of 10- to 15-year Results from Douglas-fir Thinning Experiments in the British Columbia Interior (Technical Report No. 027). British Columbia, Forest Science Program, Victoria, BC.

Keefe, R.F., Zimbelman, E.G., Picchi, G., 2022. Use of individual tree and product level data to improve operational forestry. Curr. For. Rep. 8, 148–165. https://doi.org/10.1007/s40725-022-00160-3.

Lahrsen, S., Mologni, O., Liu, Z., Röser, D., 2024. Preliminary validation of automated production analysis of feller buncher operations: integration of onboard computer data with LiDAR inventory. Eur. J. For. Res. 143, 1819–1833. https://doi.org/10.1007/s10342-024-01732-7.

Lämås, T., 2010. The Haglöf PosTex Ultrasound Instrument for the Positioning of Objects on Forest Sample Plots (Arbetsrapport No. 296). Sveriges lantbruksuniversitet: Institutionen för skoglig resurshushållning, Umeå, Sweden.

Li, J., Hu, B., Noland, T.L., 2013. Classification of tree species based on structural features derived from high density LiDAR data. Agric. For. Meteorol. 171–172, 104–114. https://doi.org/10.1016/j.agrformet.2012.11.012.

Lieffers, V.J., Pinno, B.D., Beverly, J.L., Thomas, B.R., Nock, C., 2020. Reforestation policy has constrained options for managing risks on public forests. Can. J. For. Res. 50, 855–861. https://doi.org/10.1139/cjfr-2019-0422.

Lieffers, V.J., Pinno, B.D., Johnson, A., Hossain, K.L., Gooding, T., 2023. Intensive management increases flexibility in managing wood supply. Can. J. For. Res. 53, 544–555. https://doi.org/10.1139/cjfr-2022-0317.

Martinez-Meier, A., Sanchez, L., Pastorino, M., Gallo, L., Rozenberg, P., 2008. What is hot in tree rings? The wood density of surviving Douglas-firs to the 2003 drought and heat wave. For. Ecol. Manag. 256, 837–843. https://doi.org/10.1016/j.foreco.2008.05.041.

Metsaranta, J.M., Fortin, M., White, J.C., Sattler, D., Kurz, W.A., Penner, M., Edwards, J., Hays-Byl, W., Comeau, R., Roy, V., 2024. Climate sensitive growth and yield models in Canadian forestry: challenges and opportunities. For. Chron. 100, 88–106. https://doi.org/10.5558/tfc2024-005.

Mitchell, K.J., 1988. SYLVER: modelling the impact of silviculture on yield, lumber value, and economic return. For. Chron. 64, 127–131. https://doi.org/10.5558/tfc64127b1-2.

Mologni, O., Lahrsen, S., Roeser, D., 2024. Automated production time analysis using FPDat II onboard computers: a validation study based on whole-tree ground-based harvesting operations. Comput. Electron. Agric. 222, 109047. https://doi.org/10.1016/j.compag.2024.109047.

Moreau, G., Chagnon, C., Achim, A., Caspersen, J., D'Orangeville, L., Sánchez-Pinillos, M., Thiffault, N., 2022. Opportunities and limitations of thinning to increase resistance and resilience of trees and forests to global change. For. Int. J. For. Res. 95, 595–615. https://doi.org/10.1093/forestry/cpac010.

Mulverhill, C., Coops, N.C., Wulder, M.A., Hermosilla, T., White, J.C., Bater, C.W., 2025. Projected future changes in burn probability in canada's forests and communities under different climate change scenarios. Can. J. Remote. Sens. 51, 2560347. https://doi.org/10.1080/07038992.2025.2560347.

Næsset, E., 2009. Effects of different sensors, flying altitudes, and pulse repetition frequencies on forest canopy metrics and biophysical stand properties derived from small-footprint airborne laser data. Remote. Sens. Environ. 113, 148–159. https://doi.org/10.1016/j.rse.2008.09.001.

Nigh, G.D., 2016. Total and Merchantable Volume Equations for Common Tree Species in British Columbia: by Region and Biogeoclimactic Zone (Technical Report No. 106). BC Ministry of Forests, Lands and Natural Resource Operations, Victoria, BC.

Onishi, M., Ise, T., 2021. Explainable identification and mapping of trees using UAV RGB image and deep learning. Sci. Rep. 11, 903. https://doi.org/10.1038/s41598-020-79653-9.

Parker, G.G., Russ, M.E., 2004. The canopy surface and stand development: assessing forest canopy structure and complexity with near-surface altimetry. For. Ecol. Manag. 189, 307–315. https://doi.org/10.1016/j.foreco.2003.09.001.

Pavel, M., Byrne, K., Gaudreau, J.-P., Meek, P., Belyea, D., 2021. Operational Manual for Commercial Thinning in British Columbia (Technical Report No. 93). FPInnovations, Vancouver, BC.

Penner, M., 2021. Growth and Yield Modelling Systems for BC: A Review (Technical Report). Forest Analysis and Inventory Branch, Ministry of Forests, Lands, Natural Resource Operations & Rural Development, Victoria, BC.

Pinno, B.D., Thomas, B.R., Lieffers, V.J., 2021. Wood supply challenges in Alberta – Growing more timber is the only sustainable solution. For. Chron. 97, 106–108. https://doi.org/10.5558/tfc2021-013.

Puliti, S., Lines, E.R., Müllerová, J., Frey, J., Schindler, Z., Straker, A., Allen, M.J., Winiwarter, L., Rehush, N., Hristova, H., Murray, B., Calders, K., Coops, N., Höfle, B., Irwin, L., Junttila, S., Krůček, M., Krok, G., Král, K., Levick, S.R., Luck, L., Missarov, A., Mokroš, M., Owen, H.J.F., Stereńczak, K., Pitkänen, T.P., Puletti, N., Saarinen, N., Hopkinson, C., Terryn, L., Torresan, C., Tomelleri, E., Weiser, H., Astrup, R., 2025. Benchmarking tree species classification from proximally sensed laser scanning data: Introducing the FOR-species20K dataset. Methods Ecol. Evol. 16, 801–818. https://doi.org/10.1111/2041-210X.14503.

Reid, D.E.B., Morris, D.M., Bhandari, S.K., Leitrants, C., 2025. The effects of commercial thinning treatments on the growth response of black spruce plantations in Northwestern Ontario. Can. J. For. Res. 55, 1–15. https://doi.org/10.1139/cjfr-2025-0027.

Rieder, J.S., Link, R.M., Köthe, K., Seidel, D., Ullmann, T., Žmegač, A., Zang, C., Schuldt, B., 2024. *TreeCompR*: Tree competition indices for inventory data and 3D point clouds. Methods Ecol. Evol. 15, 2198–2208. https://doi.org/10.1111/2041-210X.14414.

Riofrío, J., White, J.C., Tompalski, P., Coops, N.C., Wulder, M.A., 2022. Harmonizing multi-temporal airborne laser scanning point clouds to derive periodic annual height increments in temperate mixedwood forests. Can. J. For. Res. 52, 1334–1352. https://doi.org/10.1139/cjfr-2022-0055.

Ronoud, G., Poorazimy, M., Yrttimaa, T., Luoma, V., Huuskonen, S., Hynynen, J., Hyyppä, J., Saarinen, N., Kankare, V., Vastaranta, M., 2022. Terrestrial laser scanning in assessing the effect of different thinning treatments on the competition of scots pine (Pinus sylvestris L.) forests. Remote. Sens. 14, 5196. https://doi.org/10.3390/rs14205196.

Roussel, J.-R., Auty, D., Coops, N.C., Tompalski, P., Goodbody, T.R.H., Meador, A.S., Bourdon, J.-F., De Boissieu, F., Achim, A., 2020. lidR: an R package for analysis of airborne laser scanning (ALS) data. Remote. Sens. Environ. 251, 112061. https://doi.org/10.1016/j.rse.2020.112061.

Roussel, J.-R., Béland, M., Caspersen, J., Achim, A., 2018. A mathematical framework to describe the effect of beam incidence angle on metrics derived from airborne LiDAR: the case of forest canopies approaching turbid medium behaviour. Remote. Sens. Environ. 209, 824–834. https://doi.org/10.1016/j.rse.2017.12.006.

Roussel, J.-R., Caspersen, J., Béland, M., Thomas, S., Achim, A., 2017. Removing bias from LiDAR-based estimates of canopy height: accounting for the effects of pulse density and footprint size. Remote. Sens. Environ. 198, 1–16. https://doi.org/10.1016/j.rse.2017.05.032.

Saarinen, N., Kankare, V., Yrttimaa, T., Viljanen, N., Honkavaara, E., Holopainen, M., Hyyppä, J., Huuskonen, S., Hynynen, J., Vastaranta, M., 2020. Assessing the effects of thinning on stem growth allocation of individual Scots pine trees. For. Ecol. Manag. 474, 118344. https://doi.org/10.1016/j.foreco.2020.118344.

Sonnentag, O., Hufkens, K., Teshera-Sterne, C., Young, A.M., Friedl, M., Braswell, B.H., Milliman, T., O'Keefe, J., Richardson, A.D., 2012. Digital repeat photography for phenological research in forest ecosystems. Agric. For. Meteorol. 152, 159–177. https://doi.org/10.1016/j.agrformet.2011.09.009.

Sparks, A.M., Corrao, M.V., Keefe, R.F., Armstrong, R., Smith, A.M.S., 2024. An ACcuracy Assessment of Field and Airborne Laser Scanning–derived Individual Tree Inventories Using Felled Tree Measurements and Log Scaling Data in A Mixed Conifer Forest. For. Sci. 70, 228–241. https://doi.org/10.1093/forsci/fxae015.

Swann, D.E.B., Fried, J.S., Gray, A.N., 2025. Evaluating forest vegetation simulator (FVS) calibration options for predicting biomass accumulation across diverse Oregon landscapes. For. Ecol. Manag. 594, 122937. https://doi.org/10.1016/j.foreco.2025.122937.

Tompalski, P., Coops, N.C., White, J.C., Goodbody, T.R.H., Hennigar, C.R., Wulder, M.A., Socha, J., Woods, M.E., 2021. Estimating changes in forest attributes and enhancing growth projections: a review of existing approaches and future directions using airborne 3D point cloud data. Curr. For. Rep. 7, 1–24. https://doi.org/10.1007/s40725-021-00135-w.

Tompalski, P., Rakofsky, J., Coops, N.C., White, J.C., Graham, A.N.V., Rosychuk, K., 2019. Challenges of multi-temporal and multi-sensor forest growth analyses in a highly disturbed boreal mixedwood forests. Remote. Sens. 11, 2102. https://doi.org/10.3390/rs11182102.

Wagle, B.H., Weiskittel, A.R., Berrill, J.-P., Kizha, A.R., D'Amato, A.W., Marshall, D., 2023. Tree-level responses to commercial thinning in spruce-fir forests across northern Maine, USA. For. Ecol. Manag. 546, 121358. https://doi.org/10.1016/j.foreco.2023.121358.

Wagle, B.H., Weiskittel, A.R., Kizha, A.R., Berrill, J.-P., D'Amato, A.W., Marshall, D., 2022. Long-term influence of commercial thinning on stand structure and yield with/without pre-commercial thinning of spruce-fir in northern Maine, USA. For. Ecol. Manag. 522, 120453. https://doi.org/10.1016/j.foreco.2022.120453.

Weiskittel, A.R., Hann, D.W., Kershaw, J.A., Vanclay, J.K., 2011. Forest Growth and Yield Modeling. Wiley, Hoboken, NJ. https://doi.org/10.1002/9781119998518.

White, J.C., Tompalski, P., Bater, C.W., Wulder, M.A., Fortin, M., Hennigar, C., Robere-McGugan, G., Sinclair, I., White, R., 2025. Enhanced forest inventories in Canada: implementation, status, and research needs. Can. J. For. Res. 55, 1–37. https://doi.org/10.1139/cjfr-2024-0255.

White, J.C., Wulder, M.A., Varhola, A., Vastaranta, M., Coops, N.C., Cook, B.D., Pitt, D., Woods, M., 2013. A best practices guide for generating forest inventory attributes from airborne laser scanning data using an area-based approach. For. Chron. 89, 722–723. https://doi.org/10.5558/tfc2013-132.

Woodall, C.W., Weiskittel, A.R., 2021. Relative density of United States forests has shifted to higher levels over last two decades with important implications for future dynamics. Sci. Rep. 11, 18848. https://doi.org/10.1038/s41598-021-98244-w.

Wotherspoon, A.R., Achim, A., Coops, N.C., 2024. Assessing future climate trends and implications for managed forests across Canadian ecozones. Can. J. For. Res. 54, 278–289. https://doi.org/10.1139/cjfr-2023-0058.

Yu, X., Hyyppä, J., Kaartinen, H., Maltamo, M., 2004. Automatic detection of harvested trees and determination of forest growth using airborne laser scanning. Remote. Sens. Environ. 90, 451–462. https://doi.org/10.1016/j.rse.2004.02.001.